nanomaterials

MDPI

Article

Characteristics of p-Type Conduction in P-Doped MoS_2 by Phosphorous Pentoxide during Chemical Vapor Deposition

Jae Sang Lee, Chang-Soo Park, Tae Young Kim, Yoon Sok Kim and Eun Kyu Kim *

Department of Physics and Research Institute of Natural Sciences, Hanyang University, Seoul 04763, Korea
* Correspondence: ek-kim@hanyang.ac.kr

Received: 19 August 2019; Accepted: 5 September 2019; Published: 7 September 2019

Abstract: We demonstrated p-type conduction in MoS_2 grown with phosphorous pentoxide via chemical vapor deposition (CVD). Monolayer MoS_2 with a triangular shape and 15-μm grains was confirmed by atomic force microscopy. The difference between the Raman signals of the A_{1g} and $E^1{}_{2g}$ modes for both the pristine and P-doped samples was 19.4 cm^{-1}. In the X-ray photoelectron spectroscopy results, the main core level peaks of P-doped MoS_2 downshifted by about 0.5 eV to a lower binding energy compared to the pristine material. Field-effect transistors (FETs) fabricated with the P-doped monolayer MoS_2 showed p-type conduction with a field-effect mobility of 0.023 $cm^2/V{\cdot}s$ and an on/off current ratio of 10^3, while FETs with the pristine MoS_2 showed n-type behavior with a field-effect mobility of 29.7 $cm^2/V{\cdot}s$ and an on/off current ratio of 10^5. The carriers in the FET channel were identified as holes with a concentration of 1.01×10^{11} cm^{-2} in P-doped MoS_2, while the pristine material had an electron concentration of 6.47×10^{11} cm^{-2}.

Keywords: chemical vapor deposition; P_2O_5; p-type conduction; P-doped MoS_2

1. Introduction

Recently, various studies have analyzed two-dimensional (2D) materials, such as graphene, MoS_2, and WSe_2, because of their critical properties and abundant potential for use in optical and electrical applications [1–3]. Graphene has a zero band gap structure, but has not been able to replace semiconductor-based devices [4,5]. Additionally, layered transition metal dichalcogenides (TMDs) such as MoS_2 and WSe_2 have received enormous attention as promising materials and layer structures, in which transition metals are sandwiched between two chalcogen atom layers by a covalent force. Moreover, there are Van der Waals (VdW) forces interacting in individual layers, which make exfoliation easily. Interestingly, these materials have a unique property; their band gap structure varies depending on the thickness. In the case of MoS_2, the band gap of a monolayer has a direct band gap of 1.8 eV, while a few layers of MoS_2 and bulk MoS_2 have an indirect band gap structure with a band gap of about 1.2 eV [6].

The chemical vapor deposition (CVD) method has several advantages compared to other methods, such as mechanical and liquid exfoliation methods [7,8]. The disadvantages of the Scotch tape-based mechanical method are its difficulty in controlling the flake thickness, size, and uniformity, which makes it inappropriate for large-scale applications. The liquid method still needs to be developed for applications, while the CVD method has been used to prepare ultrathin monolayers or few-layer MoS_2 films over large areas [9]. Transistors have been fabricated via CVD growth of monolayer MoS_2. These have been reported to exhibit good properties, including a high on/off current ratio and high mobility [10]. To realize detailed applications, this method needs to be able to produce a junction composed of n- and p-type materials. Although there have been many challenges to p-type doping of

MoS_2 using niobium (Nb) or phosphorous (P) atoms [11,12], and it remains difficult to successfully dope ultrathin MoS_2. According to a previous report, P atoms seem to be the most suitable acceptors among group V elements [13].

In this paper, we report on the CVD growth and characteristics of monolayer MoS_2 with and without the addition of phosphorous pentoxide (P_2O_5) powder. The thickness and grain size of the MoS_2 layer were measured using non-contact-mode atomic force microscopy (AFM) and Raman spectroscopy. To confirm the electrical characteristics of MoS_2, back-gated field-effect transistors (FETs) were fabricated. The p-type conduction from monolayer MoS_2 grown with P_2O_5 powder was confirmed and compared to pristine MoS_2 with n-type behavior.

2. Experimental

To synthesize an MoS_2 layer by the CVD method, molybdenum trioxide (MoO_3, CERAC Inc, Milwaukee, WI, USA) powder with 99.999% purity as a precursor material and sulfur (iTASCO Inc, Seoul, Korea) powder of 99.999% purity as a reactant material were used. For p-type doping of MoS_2 in this experiment, 98.99% purity P_2O_5 (SIGMA-ALDRICH, St. Louis, MO, USA) powder was added as a dopant material. SiO_2/Si substrates (2×2 cm^2) with a SiO_2 thickness of 270 nm and three alumina boats were used. The alumina boats were filled with 10 mg of MoO_3 powder, 300 mg of S powder, and 1 mg of P_2O_5 powder, respectively. During CVD growth of MoS_2, the furnace was heated to 750 °C with a heating rate of 30 °C/min under argon gas flowing at 100 sccm. The role of argon gas was to transport S and P_2O_5 when they were vaporized. During the growth of MoS_2, the gas flow and furnace temperature were kept constant for 30 min, and then the furnace was quickly cooled down to room temperature.

The MoS_2 thickness and grain size were analyzed by using non-contact-mode atomic force microscopy (AFM) (XE-100, Park's Systems, Seoul, Korea) and optical microscopy. X-ray photoelectron spectroscopy (XPS) (K-Alpha+, Thermo Fisher Scientific, Waltham, MA, USA) under ~4×10^{-10} Torr and Raman spectroscopy (NRS-3100, JASCO, Tokyo, Japan) with a λ = 532 nm laser were measured at room temperature to identify the doping characteristics. To confirm the electrical characteristics of doped monolayer MoS_2, back-gated FETs were fabricated. In this process, photolithography was used for patterning source and drain electrodes of Ni/Au (5 nm/50 nm) metals.

3. Results

Figure 1a shows a simplified schematic diagram for the synthesis of MoS_2, with and without phosphorus doping, using the CVD system. Here, MoO_3 powder was placed in the middle of the furnace, slightly away from the S and P_2O_5 powders. The P_2O_5 powder for P doping was located about 7.5 cm from the MoO_3 powder. The ratio of S to Mo atoms is an important point for growing monolayer MoS_2 flakes. We used a face-down substrate approach, where the SiO_2 substrate is positioned vertically facing the MoO_3-containing alumina boat. Unlike previous doping studies that used a two-furnace system [14–16], this method used in situ doping with a one-furnace CVD system. The CVD process for MoS_2 growth can be divided into two steps: Nucleation and growth. Figure 1b shows the temperature profile of the reaction furnace and pressure variation in the quartz tube with Ar gas flow, respectively, as a function of time. In this figure, S atoms are introduced at 650 °C which is 100 °C lower than the growth temperature (750 °C). When S atoms are introduced, the growth of MoS_2 starts and then monolayer MoS_2 flakes appear [17].

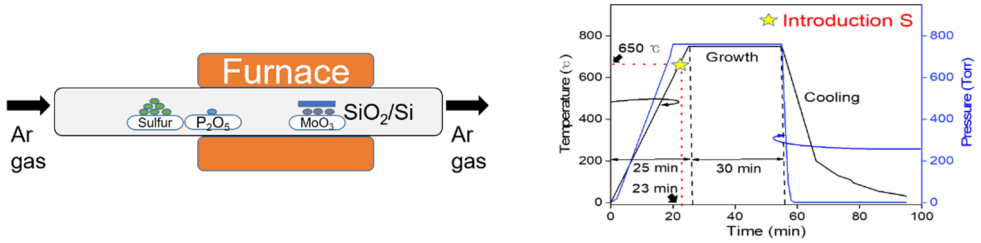

(**a**) (**b**)

Figure 1. (**a**) Schematic diagram of the chemical vapor deposition (CVD) process for the monolayer MoS_2 synthesis and in situ P doping with P_2O_5 powder. (**b**) Temperature profile of the reaction furnace and pressure in the quartz tube as a function of the processing time.

Figure 2a shows an optical microscopy image of P-doped MoS_2 grown via CVD. Here, the MoS_2 layers grown on the SiO_2/Si substrate under a sufficient S atmosphere were observed to have a triangular shape [17,18]; this is the same shape as pristine MoS_2. The grain size of doped MoS_2 on the SiO_2/Si substrate was about 15 µm. To confirm the formation of a monolayer of P-doped MoS_2, Raman spectroscopy and AFM measurements were performed, as shown in Figure 2b,c, respectively. The thickness of an MoS_2 flake measured by AFM was about 0.6 nm to 0.9 nm; this layer thickness is the same as a previous result [10]. This measurement value corresponds to the interlayer spacing of a monolayer of S-Mo-S bonding in the MoS_2 crystal. Two characteristic Raman peaks, i.e., E^1_{2g} and A_{1g} from in-plane and out-of-plane modes, respectively, were measured by a laser with an excitation wavelength of 532 nm at room temperature, as shown in Figure 2c. The in-plane E^1_{2g} mode presents the vibration of one Mo atom and two S atoms in opposite directions, while the out-of-plane A_{1g} mode vibrates only S atoms in opposite directions (as shown in the inset of Figure 2c). From reported results that describe the dependence of the Raman peaks on the number of layers [19,20], we know that the difference between two Raman peaks depending on the number of MoS_2 layers is larger than 20 cm^{-1} for thicknesses above a bilayer (2 L). As shown in Figure 2d, Raman peaks from P-doped MoS_2 were located at 384.5 cm^{-1} (E^1_{2g} mode) and 403.9 cm^{-1} (A_{1g} mode). On the other hand, the E^1_{2g} and A_{1g} signals of the pristine monolayer MoS_2 were observed at around 384.6 cm^{-1} and 405 cm^{-1}, respectively. The difference between the two Raman modes for P-doped and pristine MoS_2 (Figure 2d) appear to be about 19.4 cm^{-1} and 20 cm^{-1}, respectively; these values indicate a single layer of MoS_2.

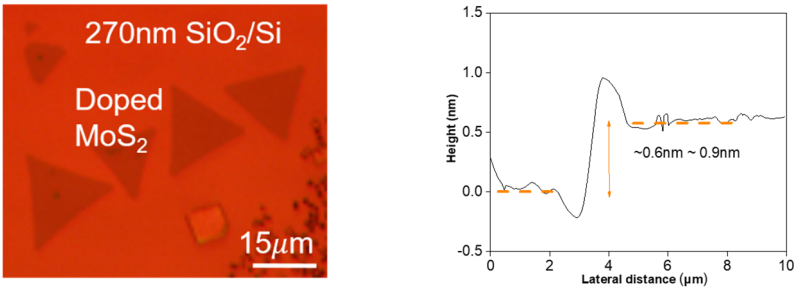

(**a**) (**b**)

Figure 2. *Cont.*

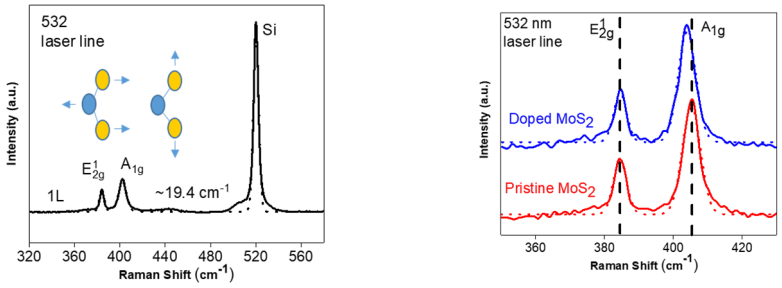

Figure 2. (**a**) Optical microscope image, (**b**) AFM height profile, and (**c**) Raman spectroscopy results using a laser with an excitation wavelength of 532 nm for a monolayer of CVD-grown MoS_2 flakes. (**d**) The two Raman modes for the pristine and doped monolayer MoS_2 flakes.

Here, the Raman signal peak of the A_{1g} mode was found to be shifted by about 1.1 cm^{-1}, while the signal peak of the $E^1{}_{2g}$ mode was almost unchanged. Azcatl et al. reported that a strain induced by dopants can generate contractions of the MoS_2 lattice structure [21]; this phenomenon occurs due to the longer bond length of Mo-S atoms than that of Mo-P atoms. It was also reported that the A_{1g} mode is often more influenced by doping effects than other modes (e.g., the $E^1{}_{2g}$ mode); this is due to its strong coupling with electrons [22,23]. Therefore, the Raman active signal with A_{1g} has a shift larger than the other Raman active signal because this peak of the Raman mode is quite sensitive to the doping effect. We confirmed that the Raman shifts in Figure 2d agreed with previous results [24]. The full width at half maximum (FHWM) of the $E^1{}_{2g}$ peak was investigated to characterize the crystalline quality of MoS_2 obtained by the CVD synthesis method. The FWHM result of the CVD-grown monolayer flake is 3.8 cm^{-1}, which is similar to a recently reported value of a CVD-synthesized single-layer flake [18].

The energy peaks appearing in XPS were also analyzed to confirm the doping properties in monolayer MoS_2 crystals. Figure 3a–c show the comparative XPS core level analyses of pristine and doped monolayer MoS_2. In Figure 3a, the P 2p binding energy peak, which clearly appears only at 134.3 eV, is associated with a doped flake feature. It is worth mentioning that the existence of this peak provides apparent evidence that P_2O_5 takes its position before the introduction of S. In addition, the Mo 3d and S 2p core levels indicated that the phenomenon causes a uniform shift of 0.5 eV, from 229.6 eV to 229.1 eV and from 162.4 eV to 161.9 eV, respectively (Figure 3b,c). That is, each peak moved toward a lower binding energy after P-doping, which is very similar to the reported results for Nb-doped MoS_2 [24]. This study reported that the Fermi level (E_F) of pristine MoS_2 is located close to the conduction band (E_c) edge, while an Nb-doped p-type sample has a Fermi level near the valence band edge. The work function and electron affinity of the pristine monolayer MoS_2 is 5.1 eV and 4.28 eV, respectively [25]. The pristine MoS_2 Fermi level is 0.82 eV, which is the E_c–E_F result, and the doping sample Fermi level is 1.32 eV, 0.82 + ΔBE (measured from XPS data). Therefore, it is suggested that doping with P_2O_5 leads to a downshift in the Fermi level of about 0.5 eV, close to the valence band maximum.

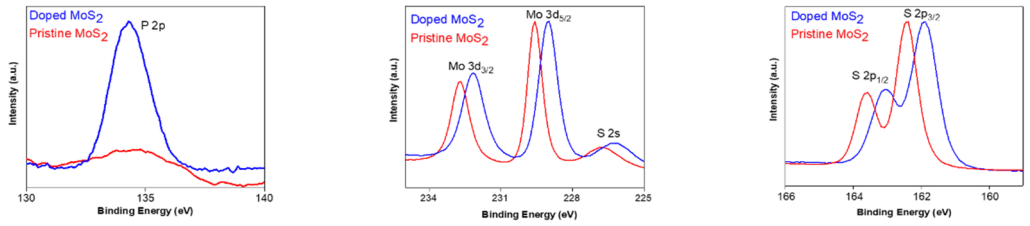

Figure 3. XPS spectra of (**a**) P 2p, (**b**) Mo 3d, and (**c**) S 2p peaks in the pristine and doped MoS_2. These results indicate that the peaks of each core level are downshifted in the doped MoS_2 flake.

Figure 4a,b show the fabricated back-gate FET schematic with a channel length of 3 μm and a channel width of 10 μm, as well as the I_{DS}–V_{DS} curve of an FET based on P-doped monolayer MoS_2, respectively.

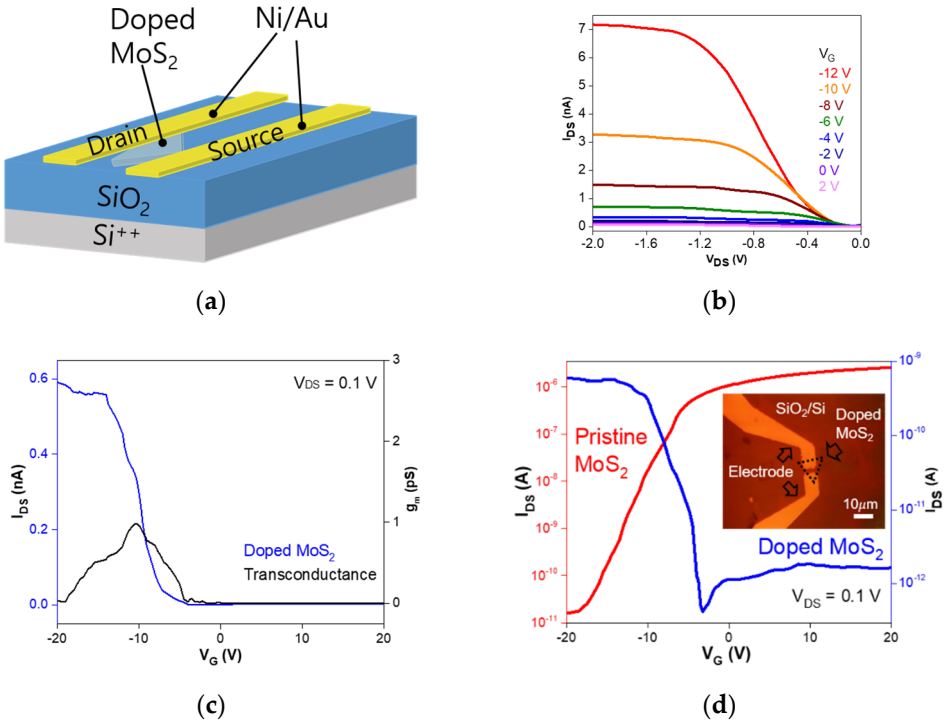

Figure 4. (**a**) Schematic of field-effect transistors (FETs) with a channel length of 3 nm and a channel width of 10 nm. (**b**) I_{DS}–V_{DS} curves of a P-doped monolayer MoS_2 FET with different gate voltages. (**c**,**d**) Linear and log scales of the transfer characteristics as a function of the gate voltage for FETs with pristine and P-doped MoS_2 channels, respectively.

Here, Ohmic metals of Ti and Ni were used for n-type pristine and p-type P-doped MoS_2 FETs, respectively, to match the metal work functions [26]. Figure 4c shows the transfer characteristics of these devices fabricated on pristine and P-doped monolayer MoS_2 flakes. The inset image of Figure 4d is the optical microscopy image of MoS_2 FETs which was fabricated on the doped monolayer MoS_2. The pristine MoS_2 FETs demonstrates n-type conduction with a high on/off current ratio of ~10^5 [27]. The threshold voltage V_T value extracted by the linear extrapolation method was about −8.1 V. In the case of P-doping, the transfer curve indicated p-type conduction with an on/off current ratio of ~10^3, and the V_T was −6.9 V at a drain-source voltage of 0.1 V. The field-effect mobilities of these FETs were calculated by the following relation:

$$\mu = (dI_{DS}/dV_{BG}) \times [L/C_{ox}\, WV_{DS}], \quad (1)$$

where L and W are the channel length and width, respectively. The back-gate capacitance ($C_{ox} = \varepsilon_0\varepsilon_r/d$) was ~$1.28 \times 10^{-8}$ F/cm^2, where ε_{0X} is the dielectric constant and d is the thickness of silicon oxide. Using the transconductance value obtained by the relation of $g_m = dI_{DS}/dV_{BG}$, the field-effect mobilities were determined to be about 29.7 cm^2/V·s and 0.023 cm^2/V·s for the pristine and P-doped MoS_2 FETs, respectively. The carrier concentration in the FET channel could also be estimated by using the following relation:

$$n = C_{ox}\,(V_{BG} - V_T)/e, \quad (2)$$

where e is the electron charge [28]. The electron concentration in pristine MoS_2 was 6.47×10^{11} cm^{-2}, whereas the hole concentration in P-doped MoS_2 was 1.01×10^{11} cm^{-2}. Based on these results, the complete p-type conduction of MoS_2 with the addition of P_2O_5 was demonstrated in this study.

4. Conclusions

We have demonstrated the p-type conduction of P-doped MoS_2 by P_2O_5 via a CVD process. Based on AFM and Raman measurements, pristine and P-doped MoS_2 were confirmed to have monolayer thickness with grain sizes in the order of 15 μm. From XPS data, it was suggested that the Fermi level of P-doped MoS_2 shifted by about 0.5 eV toward the valence band compared to the pristine MoS_2. FETs with P-doped monolayer MoS_2 showed p-type conduction with a field-effect mobility of 0.023 $cm^2/V{\cdot}s$ and an on/off current ratio of 10^3, while pristine MoS_2 FETs had n-type behavior with a field-effect mobility of 29.7 $cm^2/V{\cdot}s$ and an on/off current ratio of 10^5. The carriers in the FET channel were identified to be holes with a concentration of 1.01×10^{11} cm^{-2} in P-doped MoS_2 and electrons with a concentration of 6.47×10^{11} cm^{-2} in the pristine material. This phosphorous doping technique should be applicable to other TMD materials.

Author Contributions: J.S.L. performed the experiment, data analysis, discussed the results and wrote the paper; C.-S.P., T.Y.K. and Y.S.K. discussed the results and analyzed the data; and E.K.K. performed paper editing and supervision.

Funding: This research was supported by a National Research Foundation of Korea (NRF) grant funded by the Korean government (MSIP) (NRF-2016R1A2B4011706, NRF-2018R1A2A3074921).

Conflicts of Interest: The authors declare no conflict of interest.

References

1. Novoselov, K.S.; Geim, A.K.; Morozov, S.V.; Jiang, D.; Zhang, Y.; Dubonos, S.V.; Griorieva, I.V.; Firsov, A.A. Electric field effect in atomically thin carbon films. *Science* **2004**, *306*, 666–669. [CrossRef] [PubMed]
2. Bolotin, K.I.; Sikes, K.J.; Jiang, Z.; Klima, M.; Fudenberg, G.; Hon, J.; Kim, P.; Stormer, H.L. Ultrahigh electron mobility in suspended graphene. *Solid State Commun.* **2008**, *146*, 351–355. [CrossRef]
3. Liu, M.; Yin, X.; Ulin-Avila, E.; Geng, B.; Zentgraf, T.; Ju, L.; Wang, F.; Zhang, X. A graphene based broadband optical modulator. *Nature* **2011**, *474*, 64–67. [CrossRef] [PubMed]
4. Ozlem, S.; Akkaya, U. Graphene electronics: Thinking outside the silicon box. *Nat. Nanotechnol.* **2009**, *131*, 48–49.
5. Osada, M.; Sasaki, T. 2D inorganic nano-sheets: Two-dimensional dielectric nano-sheets: Novel nanoelectronics from nanocrystal building blocks. *Adv. Mater.* **2012**, *24*, 210–228. [CrossRef] [PubMed]
6. Gordon, R.; Yang, D.; Crozier, E.; Jiang, D.; Frindt, R. Structures of exfoliated single layers of WS_2, MoS_2, and $MoSe_2$ in aqueous suspension. *Phys. Rev. B* **2002**, *65*, 125407. [CrossRef]
7. Chu, D.; Pak, S.W.; Kim, E.K. Locally Gated SnS_2/hBN Thin Film Transistors with a Broadband Photoresponse. *Sci. Rep.* **2018**, *8*, 10585–10593. [CrossRef] [PubMed]
8. Lee, S.K.; Chu, D.; Yoo, J.; Kim, E.K. Formation of transition metal dichalcogenides thin films with liquid phase exfoliation technique and photovoltaic applications. *Sol. Energy Mater. Sol. Cells* **2018**, *184*, 9–14. [CrossRef]
9. Qiu, D.; Lee, D.U.; Pak, S.W.; Kim, E.K. Structural and optical properties of MoS_2 layers grown by successive two-step chemical vapor deposition method. *Thin Solid Films* **2015**, *587*, 47–51. [CrossRef]
10. Radisavljevic, B.; Radenovic, A.; Brivio, J.; Giacometti, V.; Kis, A. Single-layer MoS_2 transistors. *Nat. Nanotechnol.* **2011**, *6*, 147–150. [CrossRef]
11. Laskar, M.R.; Nath, D.N.; Ma, L.; Lee, E.W.; Lee, C.H.; Kent, T.; Yang, Z.; Mishra, R.; Roldan, M.A.; Idrobo, J.-C.; et al. p-type doping of MoS_2 thin films using Nb. *Appl. Phys. Lett.* **2014**, *104*, 092104. [CrossRef]
12. Momose, T.; Nakamura, A.; Daniel, M.; Shimomura, M. Phosphorous doped p-type MoS_2 polycrystalline thin films via direct sulfurization of Mo film. *AIP Adv.* **2018**, *8*, 025009. [CrossRef]
13. Dolui, K.; Rungger, I.; Pemmaraju, C.D.; Sanvito, S. Possible doping strategies for MoS_2 monolayers: Anab initiostudy. *Phys. Rev. B* **2013**, *88*, 075429. [CrossRef]

14. Xu, E.Z.; Liu, H.M.; Park, K.; Li, Z.; Losovyj, Y.; Starr, M.; Werbianskyj, M.; Fertig, H.A.; Zhang, S.X. p-Type transition-metal doping of large-area MoS_2 thin films grown by chemical vapor deposition. *Nanoscale* **2017**, *9*, 3576–3584. [CrossRef] [PubMed]
15. Zhang, K.; Bersch, B.M.; Joshi, J.; Addou, R.; Cormier, C.R.; Zhang, C.; Xu, K.; Briggs, N.C.; Wang, K.; Subramanian, S.; et al. Tuning the Electronic and Photonic Properties of Monolayer MoS_2 via In Situ Rhenium Substitutional Doping. *Adv. Funct. Mater.* **2018**, *28*, 1706950. [CrossRef]
16. Zhang, K.; Feng, S.; Wang, J.; Azcatl, A.; Lu, N.; Addou, R.; Wang, N.; Zhou, C.; Lerach, J.; Bojan, V.; et al. Manganese Doping of Monolayer MoS_2: The Substrate Is Critical. *Nano Lett.* **2015**, *15*, 6586–6591. [CrossRef]
17. Xie, Y.; Wang, Z.; Zhan, Y.; Zhang, P.; Wu, R.; Jiang, T.; Wu, S.; Wang, H.; Zhao, Y.; Nan, T.; et al. Controllable growth of monolayer MoS_2 by chemical vapor deposition via close MoO_2 precursor for electrical and optical applications. *Nanotechnology* **2017**, *28*, 084001. [CrossRef]
18. Wang, S.; Rong, Y.; Fan, Y.; Pacios, M.; Bhaskaran, H.; He, K.; Warner, J.H. Shape Evolution of Monolayer MoS_2 Crystals Grown by Chemical Vapor Deposition. *Chem. Mater.* **2014**, *26*, 6371–6379. [CrossRef]
19. Li, H.; Zhang, Q.; Yap, C.C.R.; Tay, B.K.; Edwin, T.H.T.; Olivier, A.; Baillargeat, D. From Bulk to Monolayer MoS_2: Evolution of Raman Scattering. *Adv. Funct. Mater.* **2012**, *22*, 1385–1390. [CrossRef]
20. Lee, C.G.; Yan, H.; Brus, L.E.; Heinz, T.F.; Hone, J.; Ryu, S. Anomalous Lattice Vibrations of Single-and Few-Layer MoS_2. *ACS Nano* **2010**, *4*, 2695–2700. [CrossRef]
21. Azcatl, A.; Qin, X.; Prakash, A.; Zhang, C.; Cheng, L.; Wang, Q.; Lu, N.; Kim, M.J.; Kim, J.; Cho, K.; et al. Covalent Nitrogen Doping and Compressive Strain in MoS_2 by Remote N_2 Plasma Exposure. *Nano Lett.* **2016**, *16*, 5437–5443. [CrossRef] [PubMed]
22. Chakraborty, A.; Bera, A.; Muthu, D.V.S.; Bhowmick, S.; Waghmare, U.V.; Sood, A.K. Symmetry-dependent phonon renormalization in monolayer MoS_2 transistor. *Phys. Rev. B* **2012**, *85*, 161403. [CrossRef]
23. Kukucska, G.; Koltai, J. Theoretical Investigation of Strain and Doping on the Raman Spectra of Monolayer MoS_2. *Phys. Status Solidi (B)* **2017**, *254*, 1700184. [CrossRef]
24. Suh, J.; Park, T.E.; Lin, D.Y.; Fu, D.; Park, J.; Jung, H.J.; Chen, Y.; Ko, C.; Jang, C.; Sun, Y.; et al. Doping against the native propensity of MoS_2: Degenerate hole doping by cation substitution. *Nano Lett.* **2014**, *14*, 6976–6982. [CrossRef] [PubMed]
25. Velicky, M.; Bissett, M.A.; Woods, C.R.; Toth, P.S.; Georgiou, T.; Kinloch, I.A.; Novoselov, K.S.; Dryfe, R.A. Photoelectrochemistry of Pristine Mono- and Few-Layer MoS_2. *Nano Lett.* **2016**, *16*, 2023–2032. [CrossRef] [PubMed]
26. McDonnell, S.; Addou, R.; Buie, C.; Wallace, R.M.; Hinkle, C.L. Defect-Dominated Doping and Contact Resistance in MoS_2. *ACS Nano* **2014**, *8*, 2880–2888. [CrossRef] [PubMed]
27. Zhang, Y.; Li, H.; Wang, H.; Xie, H.; Liu, R.; Zhang, S.L.; Qiu, Z.J. Thickness Considerations of Two-Dimensional Layered Semiconductors for Transistor Applications. *Sci. Rep.* **2016**, *6*, 29615–29622. [CrossRef] [PubMed]
28. Zhang, S.; Hill, H.M.; Moudgil, K.; Richter, C.A.; Walker, A.R.H.; Barlow, S.; Marder, S.R.; Hacker, C.A.; Pookpanratana, S.J. Controllable, Wide-Ranging n-Doping and p-Doping of Monolayer Group 6 Transition-Metal Disulfides and Diselenides. *Adv. Mater.* **2018**, *30*, 1802991–1802999. [CrossRef] [PubMed]